

Do unbounded bubbles ultimately become fenced inside a black hole?

F. S. Guzmán¹, L. Lehner² and O. Sarbach¹

¹*Instituto de Física y Matemáticas, Universidad Michoacana de San Nicolás de Hidalgo. Edificio C-3, Cd. Universitaria, C. P. 58040 Morelia, Michoacán, México.*

²*Department of Physics and Astronomy, Louisiana State University, 202 Nicholson Hall, Baton Rouge, Louisiana 70803-4001, USA*

We examine the dynamical behavior of recently introduced bubbles in asymptotically flat, five-dimensional spacetimes. Using numerical methods, we find that even bubbles that initially start expanding eventually collapse to a Schwarzschild-Tangherlini black hole.

I. INTRODUCTION

“Bubbles of nothing” in higher dimensional spacetimes have been the subject of significant attention in recent years. They have played a key role in understanding the phase space of black hole spacetimes in Kaluza-Klein scenarios [1, 2], have surfaced as a possible way around the black hole information paradox [3] and as mediators of non-perturbative instabilities in AdS/CFT contexts [4], been discussed in connections with orbifold decays in AdS spacetimes [5] and have been the subject of studies of bubble-bubble collisions [6, 7]. However, essentially all higher dimensional bubble studies have been presented within Kaluza-Klein scenarios as no known non-local bubble solutions outside them were available. Recent work by Copsey [8, 9] presents the first examples of bubbles in asymptotically flat and AdS cases. In particular, Ref. [9] provides data, at a moment of time symmetry, where surfaces of constant radius r are squashed three-spheres with the circumference of one of the circles converging to zero when r approaches some fixed positive value while these surfaces are metric three-spheres in the asymptotic region $r \rightarrow \infty$. By judiciously choosing the freely available geometrical variables, a “bubble of nothing” can be defined. Since Copsey’s construction gives data at a moment of time a complete picture of the spacetime is not available. While several important observations can be drawn at the hypersurface where this data is known, like the initial growth-rate of the bubble, key issues can only be addressed by examining the full evolution of the spacetime subject to the provided initial data. Among the questions one would like to answer are

- What is the bubble’s behavior in time? In particular, if a bubble begins expanding, does it keep on expanding? If the expansion were exponentially fast as in the case of Kaluza-Klein bubbles [10], the spacetime might have the ingredients for realizing a possible violation of cosmic censorship. This would occur if the bubble expanded so as to meet (a portion of) future null infinity at a finite affine time of the generators of \mathcal{I}^+ .
- If the bubble were to reverse its expansion rate, what is the end behavior? Does the bubble collapse? If so, does it form a black hole?
- If a black hole is formed, is the bubble size when the horizon forms already at the string/Planck scales? In this case the classical evolution certainly could not be trusted and string effects should be taken into account to reveal the bubble’s final fate.

In this work we examine the evolution of some of the bubble initial data presented by Copsey and answer the above questions.

Our article is organized as follows. In section II we review Copsey’s initial data representing exact bubble solutions at a moment of time symmetry. The future of this data is then obtained by solving the Cauchy problem by numerical methods. The system of evolution and constraint equations, the coordinate choices and boundary conditions used to evolve this initial data set as well as the numerical implementation are discussed in section III. In section IV we present the results of the evolutions carried out and we end in section V with a brief discussion and conclusions drawn from this work. Technicalities like the computation of the curvature tensor and curvature invariants and a summary of the Schwarzschild-Tangherlini solution can be found in the appendices.

II. PROTOTYPE METRIC AND INITIAL DATA

Recently, Copsey [9] introduced bubbles which are outside the traditionally Kaluza-Klein framework. These bubbles, for the asymptotically flat case, and at a moment of time-symmetry, are described by a $t = \text{const}$ slice of a metric of the form

$$ds^2 = -dt^2 + \frac{dr^2}{W(r)} + \frac{r^2}{4} \left[H(r) (dz + \cos \vartheta d\varphi)^2 + d\vartheta^2 + \sin^2 \vartheta d\varphi^2 \right], \quad (1)$$

where W and H are smooth functions of r which converge to 1 as $r \rightarrow \infty$ and where $(\vartheta, \varphi, z) \in [0, \pi) \times [0, 2\pi) \times [0, 4\pi)$ are Euler angles on the three-sphere S^3 . If $W \equiv H \equiv 1$, this metric describes five-dimensional Minkowski space. This can be seen by introducing the coordinates

$$x + iy = r e^{\frac{i}{2}(z-\varphi)} \sin\left(\frac{\vartheta}{2}\right), \quad X + iY = r e^{\frac{i}{2}(z+\varphi)} \cos\left(\frac{\vartheta}{2}\right),$$

in terms of which the metric (1) with $W \equiv H \equiv 1$ assumes the form

$$ds^2 = -dt^2 + dx^2 + dy^2 + dX^2 + dY^2.$$

More generally, using

$$dr = n_i dx^i, \quad dz + \cos \vartheta d\varphi = m_i dx^i,$$

where $(x^i) = (x, y, X, Y)$, $(n_i) = (x, y, X, Y)/r$ and $(m_i) = (-y, x, -Y, X)/r$, we find that

$$ds^2 = -dt^2 + h_{ij} dx^i dx^j = -dt^2 + \left[\delta_{ij} + \frac{1-W}{W} n_i n_j + (H-1) m_i m_j \right] dx^i dx^j.$$

Therefore, the metric (1) is asymptotically flat if the functions $W-1$ and $H-1$ decay to zero fast enough as $r \rightarrow \infty$. In particular, if $W = 1 - C_1/r^2 + O(r^{-3})$, $H = 1 - C_2/r^2 + O(r^{-3})$, $H' = 2C_2/r^3 + O(r^{-4})$ we obtain a finite ADM mass

$$M_{ADM} = \frac{1}{16\pi} \lim_{r \rightarrow \infty} \int_{S_r^3} \sum_{i,j=1}^4 (\partial_i h_{ij} - \partial_j h_{ii}) dS_j = \frac{\pi}{8} (3C_1 - C_2),$$

where S_r^3 denotes the three-sphere with radius r and $dS_j = n_j dS$ is the area element on S_r^3 .

Copsey's construction also assumes that the functions W and H both have a single root at some $r_0 > 0$ and are both strictly positive for $r > r_0$. This means that the circumference of the circles determined by the orbits of the Killing field ∂_z shrinks to zero at $r = r_0$. In order to understand the geometry near $r = r_0$, we replace r by the new radial coordinate

$$R = \sqrt{r^2 - r_0^2}, \quad r \geq r_0.$$

Then, the metric (1) can be rewritten as

$$ds^2 = -dt^2 + \frac{R^2 dR^2}{(R^2 + r_0^2)W} + \frac{R^2 + r_0^2}{4} \left[H (dz + \cos \vartheta d\varphi)^2 + d\vartheta^2 + \sin^2 \vartheta d\varphi^2 \right]. \quad (2)$$

Because of the assumptions on W and H , they have the form

$$\begin{aligned} W &= 2\alpha^2 \frac{r-r_0}{r_0} + O\left(\frac{r-r_0}{r_0}\right)^2 = \alpha^2 \left(\frac{R}{r_0}\right)^2 + O\left(\frac{R}{r_0}\right)^4, \\ H &= 2\beta^2 \frac{r-r_0}{r_0} + O\left(\frac{r-r_0}{r_0}\right)^2 = \beta^2 \left(\frac{R}{r_0}\right)^2 + O\left(\frac{R}{r_0}\right)^4, \end{aligned}$$

near $R = 0$, where α and β are two strictly positive constants. Therefore, as R tends to zero, the metric has the form

$$ds^2 \simeq -dt^2 + \frac{dR^2}{\alpha^2} + \frac{\beta^2}{4} R^2 (dz + \cos \vartheta d\varphi)^2 + \frac{r_0^2}{4} [d\vartheta^2 + \sin^2 \vartheta d\varphi^2].$$

Since z has period 4π , there is a conical singularity at $R = 0$ unless $\alpha\beta = 1$. If $\alpha\beta = 1$, we may replace R and z with the Cartesian coordinates (u, v) , which are defined by

$$u + iv = \frac{R}{\sqrt{\alpha}} e^{iz/2}.$$

In terms of these, the metric (2) assumes the form

$$\begin{aligned} ds^2 &= -dt^2 + du^2 + dv^2 + \frac{r_0^2 + \alpha(u^2 + v^2)}{4} [d\vartheta^2 + \sin^2 \vartheta d\varphi^2] \\ &\quad + f(u^2 + v^2)(u du + v dv)^2 + h(u^2 + v^2) [2(u dv - v du) + (u^2 + v^2) \cos \vartheta d\varphi]^2, \end{aligned}$$

where f and h are smooth functions of $u^2 + v^2$. Therefore, if $\alpha\beta = 1$, we obtain a smooth, regular asymptotically flat manifold with topology $\mathbb{R}_t \times \mathbb{R}^2 \times S^2$. At each fixed time t , the bubble is determined by the two-sphere at which the Killing field ∂_z vanishes.

A. Initial data

Data at the moment of time symmetry automatically solves the momentum constraint and one is left with having to satisfy the Hamiltonian constraint only. For a $t = \text{const}$ section of a metric of the form (1), the Hamiltonian constraint in vacuum yields

$$\left[\frac{H''}{H} + \frac{4}{r} \frac{H'}{H} - \frac{1}{2} \frac{H'^2}{H^2} + \frac{6}{r^2} \right] W + \left[\frac{1}{2} \frac{H'}{H} + \frac{3}{r} \right] W' + \frac{2}{r^2} (H - 4) = 0, \quad (3)$$

where a prime denotes differentiation with respect to r . A convenient way to solve this equation is to freely specify H and integrate the resulting linear equation for W . In order to analyze this, let H be an arbitrary smooth function with the following properties: H has a single root at some point $r = r_0 > 0$, $H(r) > 0$ for all $r > r_0$ and $H(r) = 1 - C_2/r^2 + O(r^{-3})$, $H'(r) = 2C_2/r^3 + O(r^{-4})$ and $H''(r) = -6C_2/r^4 + O(r^{-5})$ for $r \rightarrow \infty$. Furthermore, we assume that the expansion along outgoing null radial geodesics, which is proportional to $6H + rH'$, is strictly positive for all $r \geq r_0$. This condition ensures the initial data does not contain any apparent horizons [9].

For the following, it is convenient to replace the function W by a new function ζ , defined by $W(r) = H(r)(1 + \zeta(r))$, and to introduce the dimensionless compactified coordinate $s := r_0/r$ which varies from 0 to 1. Then, Eq. (3) reads

$$\frac{s}{2} (6H - sH_s) \zeta_s = (s^2 H_{ss} - 5sH_s + 6H) \zeta + [s^2 H_{ss} - 5sH_s + 8(H - 1)],$$

where the subscript s denotes differentiation with respect to s . The general solution to this equation is

$$\zeta(s) = \zeta_0(s) [C_0 + J(s)], \quad (4)$$

where C_0 is a constant and

$$\zeta_0(s) = \frac{s^2}{(6H - sH_s)^2} e^{2I(s)}, \quad J(s) = 2 \int_0^s (6H - \tau H_\tau) \frac{\tau^2 H_{\tau\tau} - 5\tau H_\tau + 8(H - 1)}{\tau^3} e^{-2I(\tau)} d\tau,$$

with

$$I(s) = \int_0^s \frac{H_\tau d\tau}{6H - \tau H_\tau}.$$

Because of the above assumptions on H , these integrals are well-defined and converge to a finite value as $s \rightarrow 1$. In particular, notice that the asymptotic behavior on H implies that $\tau^2 H_{\tau\tau} - 5\tau H_\tau + 8(H - 1) = O(\tau^3)$ so that the integrand in the expression for $J(s)$ is well-defined at $\tau = 0$. Furthermore, we see that $\zeta(s) = O(s^2)$ for small $s > 0$, hence the function W has the same asymptotic behavior as H and possesses a root at $r = r_0$. The constant C_0 is determined from the requirement of the absence of a conical singularity at $r = r_0$, $H_s(1)W_s(1) = 4$, which yields

$$C_0 = [4 - H_s(1)^2] e^{-2I(1)} - J(1).$$

Finally, we notice that without further restriction on H there is no guarantee that W is positive for all $r > r_0$. However, the condition $H < 4$ is sufficient to guarantee positivity of W for $r > r_0$. Indeed, Eq. (3) and the condition $6H + rH' > 0$ then imply that $W'(r_1) > 0$ if r_1 is a zero of W which shows that the sign of W cannot change from positive to negative when r increases.

In order to understand the initial dynamics of the bubble, we compute the initial acceleration of the bubble area \mathcal{A} with respect to proper time τ at the bubble. In terms of the general metric (A1) the bubble's area and proper time are given by

$$\mathcal{A} = 4\pi e^{2c}|_{r=r_0}, \quad d\tau = e^d dt|_{r=r_0},$$

respectively. Taking the second derivative with respect to proper time, using the evolution equation $R_{33} = 0$ in appendix A and the initial values

$$R = r, \quad a = -\frac{1}{2} \log(W), \quad b = \log\left(\frac{r}{2}\right) + \frac{1}{2} \log(H), \quad c = \log\left(\frac{r}{2}\right),$$

$\dot{a} = \dot{b} = \dot{c} = 0$ in (A1), we obtain

$$\frac{d^2 \mathcal{A}}{d\tau^2} = -2\pi W_s(1) - 8\pi = -8\pi \left[1 + \frac{1}{H_s(1)} \right]. \quad (5)$$

Therefore, the bubble starts expanding if and only if $-1 < H_s(1) < 0$. Finally, the ADM mass is

$$M_{ADM} = \frac{\pi r_0^2}{8} \left(2 \frac{C_2}{r_0^2} + \frac{C_0}{36} \right).$$

Some examples of solutions, and the ones we will employ in our simulations are

1. The choice $W = H$ simplifies Eq. (3) to the following linear equation for H ,

$$H'' + \frac{7}{r}H' + \frac{8}{r^2}(H - 1) = 0,$$

which has the general solution

$$H(r) = 1 - a_0 \left(\frac{r_0}{r} \right)^2 - a_1 \left(\frac{r_0}{r} \right)^4 \quad (6)$$

with $a_0 + a_1 = 1$. Notice that $H(r_0) = 0$ and that H can also be written in the form

$$H(r) = \left[1 - \left(\frac{r_0}{r} \right)^2 \right] \left[1 + a_1 \left(\frac{r_0}{r} \right)^2 \right]$$

from which we see that a necessary and sufficient condition for H to have a single root at r_0 and to be strictly positive for $r > r_0$ is that $a_1 > -1$, or, equivalently, $a_0 < 2$. Furthermore, H converges to one as $r \rightarrow \infty$. In order to verify the regularity condition at $r = r_0$, we compute $2\alpha^2 = r_0 H'(r_0) = 2(1 + a_1)$. Hence, $\alpha^2 = \beta^2 = 1 + a_1$ and the regularity condition $\alpha\beta = 1$ forces the choice $a_0 = 1$, $a_1 = 0$.

2. More general initial data can be obtained by employing the function H given in Eq. (6) but relaxing the condition $W = H$. In this case, the integrals in Eq. (4) can be performed analytically [9] with the result

$$\zeta(r) = c_1 \left(\frac{r_0}{r} \right)^2 \left| \frac{a_1 \left(\frac{r_0}{r} \right)^2 + a_0 - b_0}{a_1 + a_0 - b_0} \right|^{-\frac{a_0}{2b_0} - 1} \left| \frac{a_1 \left(\frac{r_0}{r} \right)^2 + a_0 + b_0}{a_1 + a_0 + b_0} \right|^{\frac{a_0}{2b_0} - 1}, \quad (7)$$

with

$$b_0 = \sqrt{a_0^2 + 3a_1}, \quad c_1 = -\frac{a_1(a_1 + 2)}{(1 + a_1)^2}.$$

If $a_1 = 0$, $\zeta \equiv 0$ and we recover the previous solution with $W = H$. However, the more general family of solutions given by H as in Eq. (6) and $W = H(1 + \zeta)$ with ζ given in Eqs. (7) allows for initially collapsing and expanding bubbles [9] since the initial acceleration is

$$\frac{d^2 \mathcal{A}}{d\tau^2} = 4\pi \frac{2a_0 - 3}{2 - a_0}. \quad (8)$$

Therefore, the bubble initially expands for $3/2 < a_0 < 2$ and initially collapses for $a_0 < 3/2$. The parameter a_0 determines the ADM mass through

$$M_{ADM} = \frac{\pi r_0^2}{8} \left[2a_0 + 3 \frac{a_1(a_1 + 2)}{(1 + a_1)^2} \left| \frac{a_0 - b_0}{a_1 + a_0 - b_0} \right|^{-\frac{a_0}{2b_0} - 1} \left| \frac{a_0 + b_0}{a_1 + a_0 + b_0} \right|^{\frac{a_0}{2b_0} - 1} \right].$$

3. A simple and interesting example is given by the choice $H(s) = (1 - s^2)^2 + \varepsilon s^2(1 - s)$, where $0 < \varepsilon < 1$. This choice satisfies all the required assumptions on H , and $0 < H(s) < 1 + \varepsilon$ for $0 \leq s < 1$. Furthermore, $H_s(1) = -\varepsilon$, so one can construct bubbles with arbitrarily large initial acceleration.
4. The following ansatz is also suggested in [9],

$$H(s) = (1 - s^2)^4 + 4\varepsilon s^2(1 - s) - \frac{4s^2(1 - s)^2 c_2}{1 + \frac{c_2}{\varepsilon}(1 - s)}, \quad (9)$$

which leads to initially hyperexpanding bubbles.

III. EVOLUTION

Here, we discuss our method for obtaining the time evolution of the time-symmetric bubble configurations discussed in the previous section. Motivated by the form (2) of the prototype metric, we perform the following rescaling in the general line element (A1)

$$d \mapsto d, \quad a \mapsto a, \quad b \mapsto b + \log\left(\frac{R}{2}\right), \quad c \mapsto c + \log\left(\frac{\sqrt{R^2 + r_0^2}}{2}\right). \quad (10)$$

The metric now takes the form

$$ds^2 = -e^{2d} dt^2 + e^{2a} dR^2 + \frac{1}{4} \left[e^{2b} R^2 (dz + \cos \vartheta d\varphi)^2 + e^{2c} (R^2 + r_0^2) d\Omega^2 \right], \quad R \geq 0. \quad (11)$$

The functions a , b , c and d which depend only on t and R must satisfy the following boundary conditions. As $R \rightarrow \infty$ we require that these functions converge to zero fast enough for quantities like the ADM mass to be defined. Near $R = 0$ we require that these functions are smooth and satisfy the conditions $a'(t, 0) = b'(t, 0) = c'(t, 0) = d'(t, 0) = 0$. Furthermore, we impose the condition $a(t, 0) - b(t, 0) = 0$ which ensures that there is no conical singularity at $R = 0$.

A. Gauge conditions

We find it convenient to impose the following family of gauge conditions on the logarithm of the lapse d ,

$$d = a + \lambda(b + 2c), \quad (12)$$

where λ is a fixed parameter. For $\lambda = 0$, this condition implies that the two-metric $-e^{2d} dt^2 + e^{2a} dR^2$ is in the conformal flat gauge. As we will see, the principal part of the evolution equations is governed by the d'Alembertian with respect to this metric. Since the two-dimensional d'Alembertian operator is conformally covariant, the resulting evolution equations are semi-linear. In particular, this implies that the characteristic speeds do not depend on the solution that is being evolved, so there cannot be shock formation due to the crossing of characteristics. When $\lambda = 1$, the gauge condition (12) is strongly related to the densitized lapse condition often encountered in hyperbolic formulations of Einstein's field equations. Indeed, the square root of the determinant of the four metric belonging to (11) is $e^{a+b+2c} R(R^2 + r_0^2) \sin \vartheta / 8$, so (12) sets the lapse e^d equal to the square root of the determinant of the four metric divided by the factor $R(R^2 + r_0^2) \sin \vartheta / 8$ which is singular at the bubble, at the poles $\vartheta = 0, \pi$ and at $R = \infty$. Since this gauge condition is essentially the time harmonic gauge condition integrated in time, it is convenient for its singularity avoidance behavior. In our simulations below, we use both choices $\lambda = 0$ and $\lambda = 1$.

B. Evolution equations

In the gauge (12), the evolution equations can be written as a coupled system of three wave equations for the fields a , b and c which are obtained from the Einstein vacuum equations $R_{11} - (\lambda + 1)G_{00} = 0$, $R_{22} = 0$ and $R_{33} = 0$, respectively. The resulting system has the form

$$\ddot{u} = e^{2\lambda(b+2c)} \left[u'' + \frac{1}{R} M u' \right] + \mathcal{F}(R, u, \dot{u}, u'),$$

where $u := (a, b, c)^T$, M is the constant 3×3 matrix

$$M = \begin{pmatrix} \lambda & -2\lambda & -2(\lambda + 1) \\ 0 & \lambda + 2 & 2(\lambda + 1) \\ 0 & 0 & 1 \end{pmatrix},$$

and \mathcal{F} is a nonlinear function of R , u , \dot{u} and u' which is regular at $R = 0$. Provided that u is smooth enough, the evolution equations are regular at $R = 0$ since then the boundary condition $u'(t, 0) = 0$ implies that

$$\lim_{R \rightarrow 0} \frac{1}{R} M u' = M u''|_{R=0}.$$

For the following, we find it convenient to replace a , b and c by the linear combinations $A = a + \lambda b + 2(\lambda + 1)c$, $B = b + 2c$ and $C = c$ which diagonalize M . Using the expressions in the appendix and taking into account the rescaling (10) we obtain

$$\begin{aligned} \ddot{A} = & \frac{1}{R^\lambda} [R^\lambda e^{2\lambda B} A']' + e^{2\lambda B} \left[-3(\lambda - 1)C'^2 + \frac{2R}{r_0^2 + R^2} (\lambda A' + 2\lambda B' - 3(\lambda - 1)C') + \frac{2(1 + \lambda)r_0^2 + (3\lambda + 1)R^2}{(r_0^2 + R^2)^2} \right] \\ & + 2\lambda \dot{A}\dot{B} - \lambda(\lambda + 1)\dot{B}^2 - 3(\lambda + 1)\dot{C}^2 + (\lambda + 3)V_0 - (\lambda + 1)V_1, \end{aligned} \quad (13)$$

$$\ddot{B} = \frac{1}{R^{\lambda+2}} e^{(\lambda-1)B} [R^{\lambda+2} e^{(\lambda+1)B} B']' + 2 \frac{e^{2\lambda B}}{r_0^2 + R^2} [(\lambda + 2)RB' + 3] + (\lambda - 1)\dot{B}^2 + 2V_0 - 2V_1, \quad (14)$$

$$\ddot{C} = \frac{1}{R} e^{(\lambda-1)B} [R e^{(\lambda+1)B} C']' + \frac{e^{2\lambda B}}{r_0^2 + R^2} [(\lambda + 1)RB' + 2RC' + 2] + (\lambda - 1)\dot{B}\dot{C} + 2V_0 - V_1, \quad (15)$$

where $V_0 = R^2(r_0^2 + R^2)^{-2} e^{2(A+B-6C)}$ and $V_1 = 4(r_0^2 + R^2)^{-1} e^{2(A-3C)}$. These equations are regular at $R = 0$ provided the boundary conditions $A' = B' = C' = 0$ at $R = 0$ are satisfied and the fields are smooth enough. Eqs. (13,14,15) are subject to the Hamiltonian constraint $\mathcal{H} = 0$ and to the momentum constraint $\mathcal{M} = 0$, where

$$\begin{aligned} \mathcal{H} &\equiv -e^{2d} G_{00} \\ &= \frac{e^{(\lambda-1)B}}{R^{\lambda+2}} [R^{\lambda+2} e^{(\lambda+1)B} B']' - e^{2\lambda B} \left[\frac{1}{R} A' + A'B' - 3C'^2 + \frac{2R}{r_0^2 + R^2} (A' - (\lambda + 1)B' - 3C') - \frac{4r_0^2 + 3R^2}{(r_0^2 + R^2)^2} \right] \\ &\quad - \dot{A}\dot{B} + \lambda\dot{B}^2 + 3\dot{C}^2 + V_0 - V_1, \end{aligned} \quad (16)$$

$$\begin{aligned} \mathcal{M} &\equiv -e^{2d} R_{01} \\ &= e^{\lambda B} \left[\dot{B}' - \dot{A}B' - \dot{B}(A' - (\lambda + 1)B') + 6\dot{C}C' - \frac{1}{R} (\dot{A} - (\lambda + 1)\dot{B}) - \frac{2R}{r_0^2 + R^2} (\dot{A} - \lambda\dot{B} - 3\dot{C}) \right]. \end{aligned} \quad (17)$$

Notice that

$$\lim_{R \rightarrow 0} R\mathcal{M} = -e^{\lambda B} \left(\dot{A} - (\lambda + 1)\dot{B} \right) \Big|_{R=0}, \quad (18)$$

hence the satisfaction of the momentum constraint implies the condition $a(t, 0) - b(t, 0) = A(t, 0) - (\lambda + 1)B(t, 0) = 0$ for the avoidance of the conical singularity at $R = 0$. In the next subsection, we show that the evolution equations and the regularity conditions $A'(t, 0) = B'(t, 0) = C'(t, 0) = 0$ imply that the constraints $\mathcal{H} = \mathcal{M} = 0$ are satisfied everywhere and at each time if satisfied initially.

C. Propagation of the constraints

As a consequence of the twice contracted Bianchi identities (see appendix A) and the evolution equations which imply $G_{11} = G_{00}$, $G_{22} = G_{33} = G_{44} = -\lambda G_{00}$ we find that the constraint variables \mathcal{H} and \mathcal{M} obey the following linear evolution system

$$\dot{\mathcal{H}} = (3\lambda - 1)\dot{B}\mathcal{H} + e^{\lambda B} \left[\mathcal{M}' + \left(B' + \frac{r_0^2 + 3R^2}{R(r_0^2 + R^2)} \right) \mathcal{M} \right], \quad (19)$$

$$\dot{\mathcal{M}} = (2\lambda - 1)\dot{B}\mathcal{M} + e^{\lambda B} \left[\mathcal{H}' + (1 + \lambda) \left(B' + \frac{r_0^2 + 3R^2}{R(r_0^2 + R^2)} \right) \mathcal{H} \right]. \quad (20)$$

This system can be simplified by introducing the rescaled variables

$$\tilde{\mathcal{H}} := R(r_0^2 + R^2)e^B \mathcal{H}, \quad \tilde{\mathcal{M}} := R(r_0^2 + R^2)e^B \mathcal{M}.$$

In terms of these, the constraint propagation system reads

$$\dot{\tilde{\mathcal{H}}} = 3\lambda\dot{B}\tilde{\mathcal{H}} + e^{\lambda B}\tilde{\mathcal{M}}', \quad (21)$$

$$\dot{\tilde{\mathcal{M}}} = 2\lambda\dot{B}\tilde{\mathcal{M}} + e^{\lambda B} \left[\tilde{\mathcal{H}}' + \lambda \left(B' + \frac{r_0^2 + 3R^2}{R(r_0^2 + R^2)} \right) \tilde{\mathcal{H}} \right]. \quad (22)$$

Notice that the regularity conditions $A'(t, 0) = B'(t, 0) = C'(t, 0) = 0$ at $R = 0$ imply that $\lim_{R \rightarrow 0} \tilde{\mathcal{H}} = 0$ and that $\lim_{R \rightarrow 0} \tilde{\mathcal{M}}$ exists. Therefore, Eqs. (21,22) are regular at $R = 0$. Defining the following “energy” norm for the constraint variables

$$\mathcal{E}(t) := \frac{1}{2} \int_0^\infty (\tilde{\mathcal{H}}^2 + \tilde{\mathcal{M}}^2) R^\lambda (r_0^2 + R^2)^\lambda dR,$$

taking a time derivative and using Eqs. (21,22) we obtain

$$\frac{d}{dt} \mathcal{E} = R^\lambda (r_0^2 + R^2)^\lambda e^{\lambda B} \tilde{\mathcal{H}} \tilde{\mathcal{M}} \Big|_{R=0}^\infty + \lambda \int_0^\infty \dot{B} (3\tilde{\mathcal{H}}^2 + 2\tilde{\mathcal{M}}^2) R^\lambda (r_0^2 + R^2)^\lambda dR. \quad (23)$$

The boundary term on the right-hand side vanishes because of the regularity conditions at $R = 0$ and under the assumption that all fields fall off sufficiently fast as $R \rightarrow \infty$. If the quantity \dot{B} is bounded, we can estimate the integral term on the right-hand side by a constant K times the energy norm \mathcal{E} , and we obtain an estimate of the form

$$\mathcal{E}(t) \leq e^{|\lambda|Kt} \mathcal{E}(0).$$

This shows that if the constraints are satisfied initially, they are also satisfied for all $t > 0$ for which a smooth enough solution to the evolution equations exists. More generally, this inequality shows that convergence of $\mathcal{E}(0)$ to zero implies that $\mathcal{E}(t)$ also converges to zero for each such t . This is important for the numerical implementation below where the initial data does not satisfy the constraints exactly due to truncation errors, but where the initial constraint violation converges to zero with increasing resolution. Finally, we notice that in the particular gauge where $\lambda = 0$ the “energy” norm \mathcal{E} cannot grow in time.

D. Outer boundary conditions

In our numerical implementation below, we truncate the domain at some large radius $R_{max} \gg r_0$ and impose the following boundary conditions at $R = R_{max}$. First, we enforce the momentum constraint $\mathcal{M}|_{R=R_{max}} = 0$, which yields the boundary condition

$$\dot{B}' \Big|_{R=R_{max}} = \left[\dot{A}B' + \dot{B}(A' - (\lambda + 1)B') - 6\dot{C}C' + \frac{1}{R} (\dot{A} - (\lambda + 1)\dot{B}) + \frac{2R}{r_0^2 + R^2} (\dot{A} - \lambda\dot{B} - 3\dot{C}) \right] \Big|_{R=R_{max}}. \quad (24)$$

When estimating the constraint errors, ∞ has to be replaced by R_{max} in the expression for $\mathcal{E}(t)$ above. One then obtains the same equality as in Eq. (23) but with ∞ replaced by R_{max} on the right-hand side of that equation. The enforcing of the momentum constraint then guarantees that the boundary term vanishes. Therefore, we conclude as before that the constraint errors converge to zero at each fixed $t > 0$ if the initial constraint errors converge to zero.

Finally, we impose a Sommerfeld-like boundary condition on the fields A and C ,

$$\dot{A} + e^{\lambda B} A' \Big|_{R=R_{max}} = 0, \quad \dot{C} + e^{\lambda B} C' \Big|_{R=R_{max}} = 0. \quad (25)$$

These two boundary conditions set the incoming characteristic fields corresponding to the evolution equations for A and C to zero, and thus do absorb high-frequency outgoing waves. However, these boundary conditions do yield reflections for low-frequency waves propagating towards large R . In our simulations below, we choose R_{max} to be large enough so that such reflections do not influence the region where physics is extracted.

E. Numerical implementation

In order to numerically implement the evolution system (13,14,15) we find it convenient to rewrite it as a first order symmetric hyperbolic system by introducing the variables $\pi_A := \dot{A}$, $\pi_B := \dot{B}$, $\pi_C := \dot{C}$ and $\psi_A := A'$, $\psi_B := B'$, $\psi_C := C'$. The resulting system has the form

$$\dot{u} = \pi, \quad (26)$$

$$\dot{\pi} = e^{2\lambda B} E^{-1} \frac{d}{dR} (E\psi) + F(u, \pi, \psi; R), \quad (27)$$

$$\dot{\psi} = \frac{d}{dR} \pi, \quad (28)$$

where $u = (A, B, C)$, $\pi = (\pi_A, \pi_B, \pi_C)$, $\psi = (\psi_A, \psi_B, \psi_C)$, $E = \text{diag}(R^\lambda e^{2\lambda B}, R^{\lambda+2} e^{(\lambda+1)B}, R e^{(\lambda+1)B})$ and $F(u, \pi, \psi; R)$ is a nonlinear term that can be read off from Eqs. (13,14,15). This system is then discretized by the method of lines. Let us start with the description of our spatial discretization.

We consider first a uniform grid $R_j = j\Delta R$, $j = 0, 1, 2, \dots, N$, where $\Delta R > 0$ is a fixed mesh size, and replace the functions u , π and ψ with gridfunctions u_j , π_j and ψ_j , $j = 0, 1, 2, \dots, N$, respectively. The evolution system (26,27,28) is then approximated by the semi-discrete system

$$\dot{u}_j = \pi_j, \quad (29)$$

$$\dot{\pi}_j = e^{2\lambda B_j} E_j^{-1} D(E\psi)_j + F(u, \pi, \psi; R_j), \quad j = 1, 2, \dots, N, \quad (30)$$

$$\dot{\psi}_j = (D\pi)_j, \quad (31)$$

where D denotes the finite differencing operator

$$(D\pi)_j = \begin{cases} \frac{\pi_{j+1} - \pi_{j-1}}{2\Delta R}, & j = 1, 2, \dots, N-1, \\ \frac{\pi_j - \pi_{j-1}}{\Delta R}, & j = N, \end{cases}$$

which is second order accurate in the interior points $j = 1, 2, \dots, N-1$ and first order accurate at the exterior point $j = N$. At the inner point $j = 0$, we use the regularity condition $\psi(t, 0) = 0$ and assume smoothness of ψ , which imply

$$\lim_{R \rightarrow 0} E^{-1} \frac{d}{dR} (E\psi) = \Lambda \frac{d\psi}{dR}, \quad \Lambda = \text{diag}(\lambda + 1, \lambda + 3, 2)$$

by de L'Hôpital's rule. We then evolve u_0 , π_0 and ψ_0 according to

$$\dot{u}_0 = \pi_0, \quad (32)$$

$$\dot{\pi}_0 = e^{2\lambda B_0} \Lambda \frac{\psi_1}{\Delta R} + F(u, \pi, \psi; 0), \quad (33)$$

$$\dot{\psi}_0 = 0. \quad (34)$$

In order to impose the outer boundary conditions (24,25) we replace $(\dot{\psi}_B)_N$ by

$$(\dot{\psi}_B)_N = \left[\pi_A \psi_B + \pi_B (\psi_A - (\lambda + 1) \psi_B) - 6\pi_C \psi_C + \frac{1}{R} (\pi_A - (\lambda + 1) \pi_B) + \frac{2R}{r_0^2 + R^2} (\pi_A - \lambda \pi_B - 3\pi_C) \right]_N$$

and apply Olsson's projection method [11] in order to incorporate the Sommerfeld-type conditions (25). This method consists in applying the projector

$$P = \frac{1}{2} \begin{pmatrix} 1 & -e^{\lambda B} \\ -e^{-\lambda B} & 1 \end{pmatrix}$$

to the two-vectors $(\dot{\pi}_A, \dot{\psi}_A)_N$ and $(\dot{\pi}_C, \dot{\psi}_C)_N$. The projected fields then satisfy

$$(\dot{\pi}_A)_N + e^{\lambda B_N} (\dot{\psi}_A)_N = 0, \quad (\dot{\pi}_C)_N + e^{\lambda B_N} (\dot{\psi}_C)_N = 0,$$

which agrees with (25) in the high-frequency approximation.

In our simulations, we choose units in which $r_0 = 1$. In order to improve the accuracy of our code, we replace the radial coordinate R by a computational coordinate x with

$$R = \frac{x}{1 - k \frac{x}{x_{max}}}, \quad 0 \leq x \leq x_{max}, \quad (35)$$

where $0 \leq k < 1$ is a "stretching" parameter. A uniform grid $x_j = j\Delta x$, $j = 0, 1, 2, \dots, N$ in x is then used, where $\Delta x = x_{max}/N$. Since $dR = dx/(1 - kx/x_{max})^2$, a uniform grid in x implies (for $k > 0$) a non-uniform grid for R , with a smaller mesh size near the bubble than near the outer boundary. Since the fields have their largest gradient near the bubble, this non-uniformity in R helps better resolve the dynamics. Typically, we use the values $x_{max} = 10$ and $k = 0.8$ in our simulations which implies that R_{max} is fifty times as large as r_0 .

Next, we use a third order Runge-Kutta algorithm in order to perform the time integration. In our simulations, we use 0.2 as a value for the Courant-Friedrichs-Levy factor $\Delta t/\Delta x$. In [12] we have shown for a related model problem

consisting of the reduced wave equation for spherically symmetric solutions that this discretization leads to a stable and convergent scheme.

Finally, initial data for u , π and ψ is obtained by comparing the metrics (2) and (11). This yields

$$A = a + \lambda b, \quad B = b, \quad C = 0, \quad \psi_A = \frac{da}{dR} + \lambda \frac{db}{dR}, \quad \psi_B = \frac{db}{dR}, \quad \psi_C = 0,$$

and $\pi_A = \pi_B = \pi_C = 0$, where

$$a = -\frac{1}{2} \log(W/R^2) - \frac{1}{2} \log(r_0^2 + R^2), \quad b = \frac{1}{2} \log(H/R^2) + \frac{1}{2} \log(r_0^2 + R^2),$$

and where we recall that W/R^2 and H/R^2 converge to a finite value as $R \rightarrow 0$.

IV. RESULTS

The numerical evolution of the initial data discussed in section II suggest that the bubble eventually collapses to the Schwarzschild-Tangherlini solution, regardless whether or not the bubble is initially expanding or collapsing. This is shown in detail in the following subsections.

A. Evolution of the bubble area

In Fig. 1 we show the typical dynamical behavior of the bubble for type 2 and 4 initial data. More specifically, we show the bubble's area as a function of proper time at the bubble. It can be seen that even for type 4 initial data configurations with a violent initial expansion the bubble finally collapses in a finite proper time. We also explored a wider range of values for the parameters a_0 and ε , also evolved type 3 initial data and found that the result is the same in all cases: the bubble area shrinks to zero after a finite proper time.

The numerical parameters used in these calculations are: $R_{max} = 50$, $k = 0.8$, $N = 1000$. In the case of the type 2 data, we use the gauge condition (12) with $\lambda = 1$. Because of the singularity avoidance property of this gauge condition, we are able to continue the evolution for some time after the bubble area has shrunk to zero and are able to follow the evolution for long enough time to observe the formation of an apparent horizon and its settling down to an equilibrium black hole (see next subsection). However, for the evolution of type 4 data we observe the development of large gradients in the derivatives of the fields, similar to those found in a shock formation situation. This happens before the turning point in the evolution of the bubble area and we are unable to continue the evolution. For this reason we choose the gauge condition (12) with $\lambda = 0$ instead. As mentioned above the evolution equations are semilinear in this case, and thus there cannot be shocks due to crossing of characteristics.

B. Formation of an apparent horizon

In order to provide evidence for the bubble settling down to the Schwarzschild-Tangherlini solution, we first check whether an apparent horizon forms. This is done by calculating the expansion of the outgoing null normal defined as $l^a = n^a + s^a$ with n^a the future-directed timelike normal to the $t = \text{const}$ hypersurface and s^a the outward pointing unit normal to the surfaces $R = \text{const}$ which is orthogonal to n^a . For the $t = \text{const}$ surfaces of the metric (A1) the expansion reduces to

$$\theta = e^{-a} (b' + 2c') + e^{-d} (\dot{b} + 2\dot{c}).$$

In terms of our main evolution variables (i.e. after the rescaling of the lower case variables, and then the redefinition in terms of the upper case ones), this can be reexpressed as

$$e^{A-2C} \theta = e^{\lambda B} \left(B' + \frac{3R^2 + r_0}{R(R^2 + r_0)} \right) + \dot{B}.$$

The apparent horizon is determined by the outermost surface defined by $\theta = 0$. Since the factor e^{A-2C} is positive, it can be ignored for our purposes.

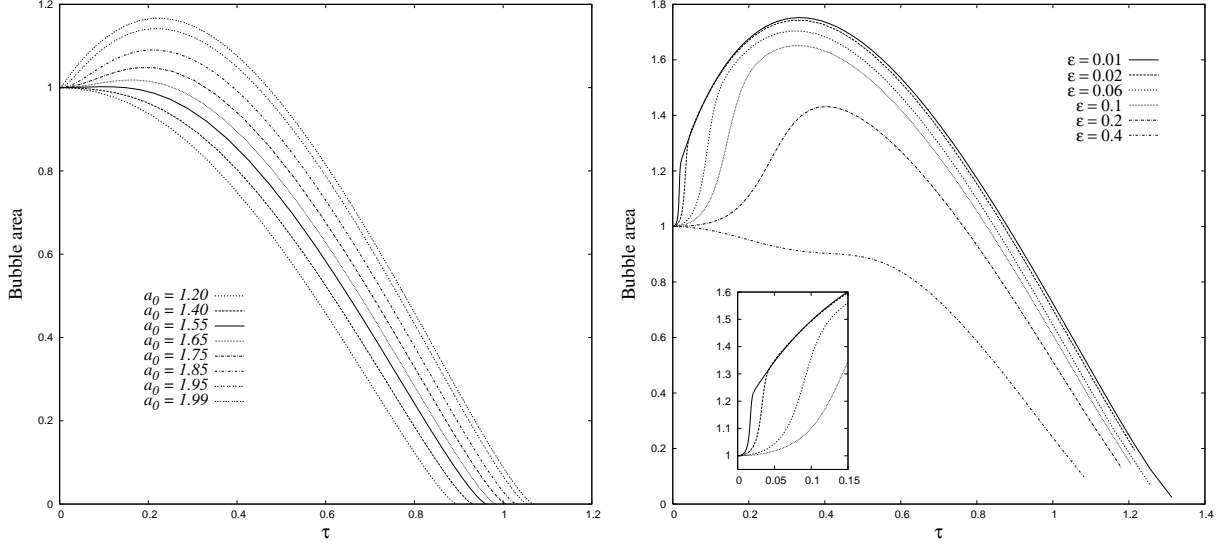


FIG. 1: We show the bubble area (normalized by its initial area) versus proper time evaluated at the bubble. Left: evolution of initial data of type 2 with several choices for the initial parameter a_0 . Right: evolution of type 4 initial data for $c_2 = 1$ and different values of the parameter ε . The inset shows an initial violent expansion of the bubble area. Nevertheless, this behavior changes and the bubble starts decelerating. In all cases the area shrinks to zero after a finite proper time.

After detecting an apparent horizon we evaluate the curvature invariants I_N , J_N and K_N defined in appendix B where we replace r_{EH} by the apparent horizon radius r_{AH} defined as the areal radius of the $t = \text{const}$ cross sections of the apparent horizon,

$$r_{AH} := [R(r_0^2 + R^2)e^B]^{1/3}. \quad (36)$$

In order to check that the horizon is $SO(4)$ symmetric, we also compute the quantity

$$\mu := \frac{e^{2b} - e^{2c}}{e^{2b} + e^{2c}} = \frac{R^2 e^{2(B-2C)} - (R^2 + r_0^2) e^{2C}}{R^2 e^{2(B-2C)} + (R^2 + r_0^2) e^{2C}},$$

on the apparent horizon. This quantity measures how close a given three-surface $t = \text{const}$, $R = \text{const}$, is of being a metric S^3 . In particular, $\mu = 0$ if this surface is a metric (unsquashed) S^3 .

The time evolution of the invariants I_N , J_N , K_N and μ are shown in Fig. 2 for two different values of the parameter a_0 for type 2 initial data. It can be seen that I_N , J_N and K_N converge to 1 and that μ converges to zero, which is a strong indication that the apparent horizon settles down to the event horizon of the Schwarzschild-Tangherlini solution. The numerical parameters used in these calculations are: $R_{max} = 50$, $k = 0.8$, $N = 4000$, $\lambda = 1$. For type 4 initial data, where we need to use the gauge choice (12) with $\lambda = 0$ in order to get to the collapse, we are able to detect the formation of an apparent horizon, but after that we soon have to stop the simulation because the resulting gauge condition is not singularity avoiding. In order to track the late time behavior of the invariants we switch from $\lambda = 0$ to $\lambda = 1$ shortly after the bubble starts collapsing. We then observe the same qualitative features as for type 2 initial data: an apparent horizon forms and the curvature invariants I_N , J_N and K_N converge to one and μ to zero. Therefore, it seems that in this case too the solution settles down to a Schwarzschild-Tangherlini black hole.

As indicated, all cases explored where the bubbles begin expanding turn around and eventually collapse. This collapse is hidden however from external observers by the appearance of an event horizon before the bubble shrinks to zero size. An important issue to examine is the size of the bubble when a horizon forms as if it were significantly smaller than the bubble's initial size string effects would become relevant and the present classical analysis would not apply. To examine this behavior we consider the type 2 data family of initially expanding bubbles and obtain the size of the bubble when an apparent horizon first appears. The results (shown in table I) indicate that the bubble only shrinks to about 1/3 of its initial size by the time the horizon forms. Therefore, a "classically-sized" bubble would seem to form a horizon while itself is still in the classical regime as suggested by its apparent horizon size. Certainly one should be careful with this argument since the apparent horizons are slicing-dependent. However, by monitoring the behavior of null rays one can also study the formation of an event horizon and the overall causal structure of the resulting spacetime. To this end we trace past-directed ingoing null rays from a late-time slice of our simulation.

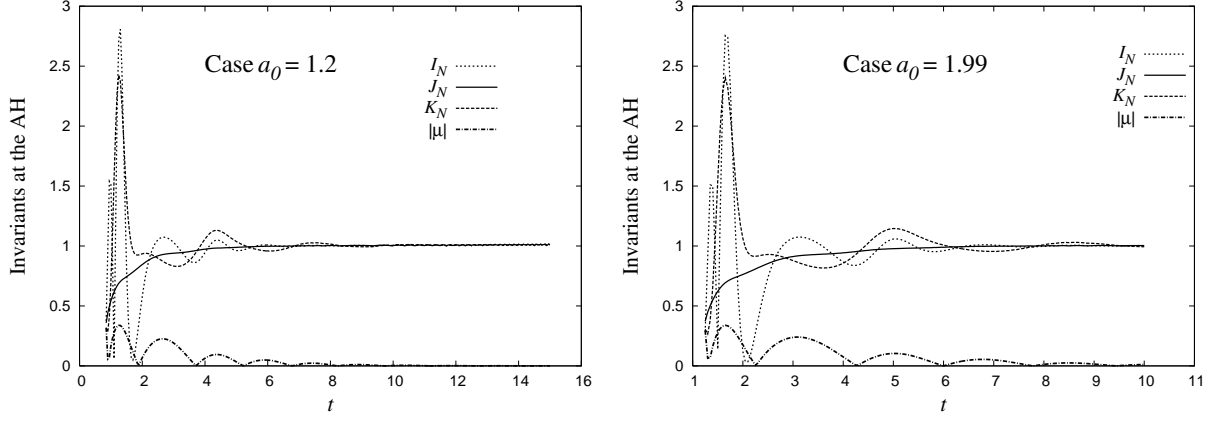


FIG. 2: The time evolution of the invariants I_N , J_N , K_N and μ for type 2 initial data with two different values of a_0 . The apparent horizon forms at a time between $t = 0.8$ and 0.85 in the case with $a_0 = 1.2$ and at a time between $t = 1.25$ and 1.3 for $a_0 = 1.99$.

This is shown in Fig. 3 for the type 2 initial data with $a_0 = 1.99$. As seen from the plot, the event horizon does not intersect the initial hypersurface but branches off the bubble shortly after the bubble reaches its maximum size. We would like to mention that while the results discussed above, and the ones included in the table illustrate what is observed for the case of type 2 initial data, a similar behavior is obtained for the other data types discussed.

| a_0 | 1.55 | 1.65 | 1.75 | 1.85 | 1.95 | 1.99 |
|-------------|------|------|------|------|------|------|
| Bubble size | 0.27 | 0.27 | 0.28 | 0.29 | 0.29 | 0.29 |

TABLE I: Size of the bubble when the apparent horizon first appears for different values of the initial data parameter a_0 .

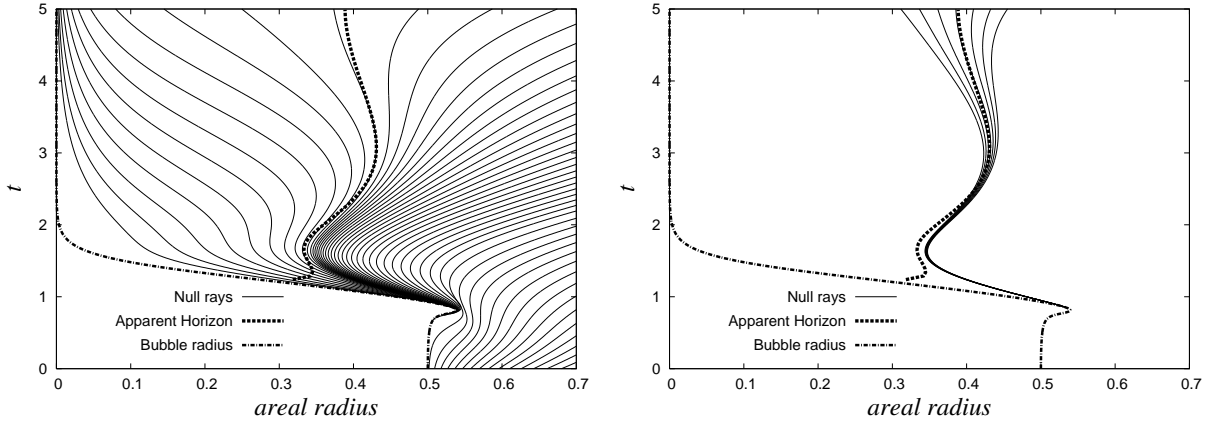


FIG. 3: Left: the past-directed ingoing null rays for the numerical spacetime obtained from type 2 initial data with $a_0 = 1.99$. The dotted line corresponds to the location of the apparent horizon and the dotted-dashed line indicates the location of the bubble area. Right: only a small subset of rays near the location of the apparent horizon is shown. This indicates that an event horizon forms at the bubble shortly after the bubble reaches its maximum size. As can be seen, the apparent horizon at late times $t \gtrsim 2.5$ is a good approximation for the event horizon. Here, time t refers to coordinate time and not proper time as in Fig. 1 and the areal radius refers to the geometric radius of the two-spheres which is equal to $e^C \sqrt{R^2 + r_0^2}/2$. Although not apparent from the plot, we have verified that the area of the S^3 cross sections of the event horizon does grow in time, as expected from the area theorem [13].

Further insight of the spacetime behavior can be obtained by comparing the ADM mass with the irreducible mass of the formed horizon. In Fig. 4 we compare the ADM mass with the apparent horizon mass of the final black hole which is defined as $M_{AH} = \frac{3\pi}{8} r_{AH}^2$ where r_{AH} is the apparent horizon radius defined in Eq. (36). The ADM mass is determined from the parameter a_0 in the initial data [9]. The difference between the two masses indicates

that significant radiation is produced during the collapse of the bubble. The numerical parameters used in these calculations are: $R_{max} = 50$, $k = 0.8$, $N = 4000$, $\lambda = 1$.

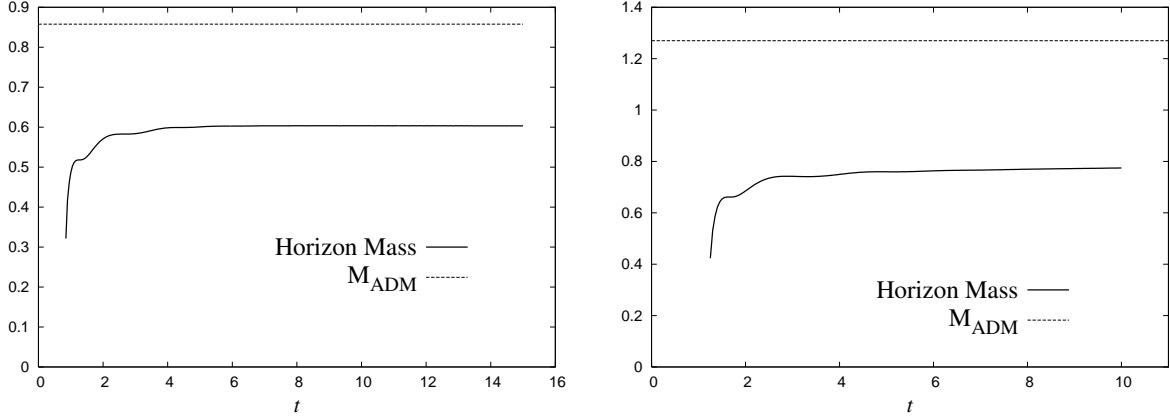


FIG. 4: The M_{ADM} and horizon masses vs time are shown for the cases $a_0 = 1.2$ (left) and $a_0 = 1.99$ (right).

C. Convergence checks

In order to verify the convergence of our numerical approximation we performed several tests. First, we verify that the constraint errors become smaller as resolution is increased. This is shown in Figs. 5 and 6 for type 2 initial data with two different values of a_0 . In these figures, we compute the quantity $CV = \sqrt{H_\infty^2 + M_\infty^2}$ where

$$H_\infty := \max_{1 \leq j \leq N} \frac{R_j}{\sqrt{1 + R_j^2}} \mathcal{H}_j, \quad M_\infty := \max_{1 \leq j \leq N} \frac{R_j}{\sqrt{1 + R_j^2}} \mathcal{M}_j.$$

As Figs. 5 and 6 indicate, the constraint errors show second order convergence to zero as resolution is increased. The numerical parameters used in these calculations are: $R_{max} = 50$ and $k = 0.8$.

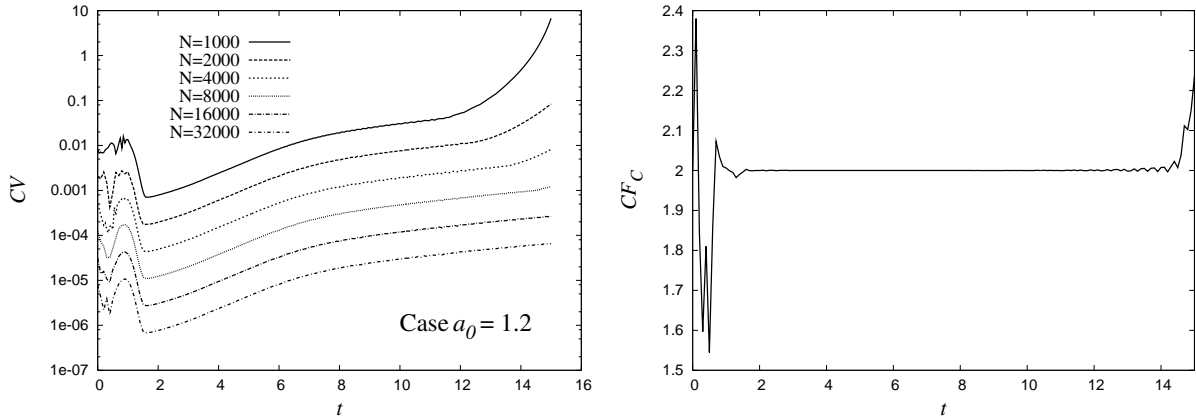


FIG. 5: Left: the quantity $CV = \sqrt{H_\infty^2 + M_\infty^2}$ vs time for various resolutions, for the value $a_0 = 1.2$. Right: the convergence factor CF_C vs time. This factor is defined as $CF_C := \log_2(CV(N = 8000)/CV(N = 16000))$.

Next, we also perform a self-convergence test for the field A . This is shown in Fig. 7 which indicates second order convergence.

We also find convergence for type 3 and type 4 initial data although the corresponding convergence factors sometimes drop well below two in those cases, though remains above 1. This drop is due to the large gradients appearing in these solutions.

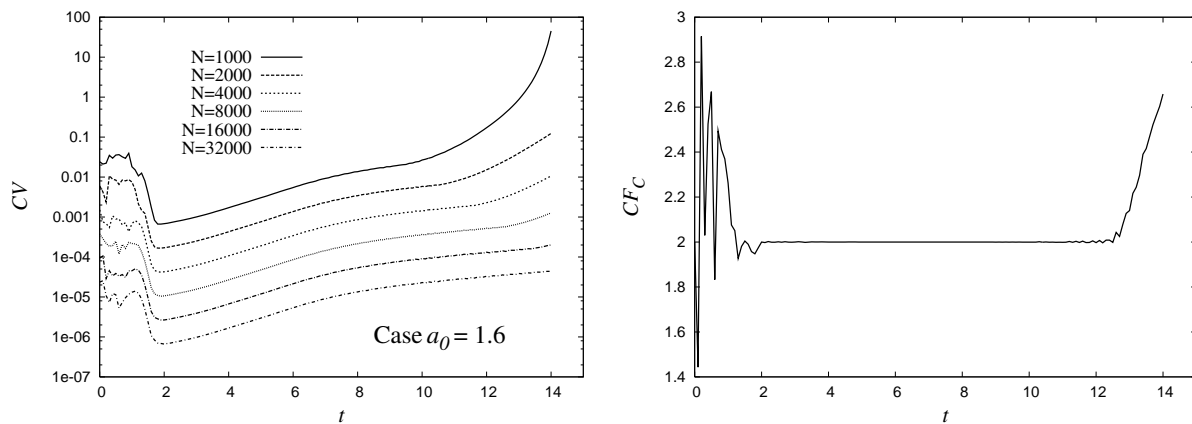


FIG. 6: The same as in the previous figure, but for the value $a_0 = 1.6$.

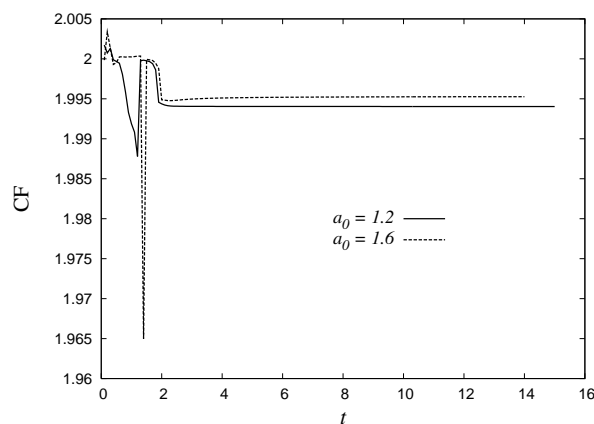


FIG. 7: Convergence factor CF vs time for the case $a_0 = 1.6$. This factor is defined as $CF = \log_2(\|A(N = 8000) - A(N = 16000)\|_\infty / \|A(N = 16000) - A(N = 32000)\|_\infty)$, where $\|A\|_\infty$ denotes the maximum value of A on the computational grid. The fact that CF is nearly equal two confirms second order convergence of our code.

V. CONCLUSIONS

In this work we examined the behavior of families of bubbles of nothing in five-dimensional asymptotically flat spacetimes. The simulations carried out reveal that independent of their initial behavior, these bubbles eventually collapse and form a black hole horizon around them. The formation of the horizon takes place at a time when the bubble's size is of the order of its initial size. Hence, starting with a ‘classically-sized’ bubble, the collapse and black hole formation occurs well above the string/Planck length. Thus, at least for the family considered, cosmic censorship is not violated and the overall process takes place at a classical level. The singularity that eventually forms in the spacetime is likely the same as that of the Tangherlini solution, thus its black hole singularity resolution at the quantum level should apply to this case as well. The behavior of initially expanding bubbles examined in this work is in sharp contrast with those with the same initial behavior in the Kaluza-Klein picture [10]. There the expansion continues and increases as time progresses and ultimately its expansion rate approaches light-speeds. This observation seems to indicate the presence of a fundamental underlying effect causing the turn-around in the asymptotically flat case. However, we want to stress that our analysis has not covered all asymptotically flat bubble solutions presented by Copesey and that we have not examined the AdS case. It would be extremely interesting to know whether the behavior found here is generic.

VI. ACKNOWLEDGMENTS

We would like to thank K. Copsey for many stimulating discussions and for making available his results prior to publication. We also want to thank Vijay Balasubramanian, Robert Myers, Jorge Pullin and Thomas Zannias for useful discussions. Last we wish to thank Jorge Pullin for bringing this problem to our attention. This work was supported in part by grants from NSF: PHY-0326311 and PHY-0554793 to Louisiana State University, by grants CIC: 4.9 and 4.20 to Universidad Michoacana and PROMEP: UMICH-PTC-121, UMSNH-CA-22 from SEP Mexico. L.L. thanks CIAR for support and is grateful to the Research Corporation for financial support. O.S. thanks Louisiana State University for its hospitality.

APPENDIX A: EXPRESSIONS FOR THE CURVATURE TENSOR

In this appendix we compute the curvature and Ricci tensors belonging to the metric

$$ds^2 = -e^{2d}dt^2 + e^{2a}dR^2 + e^{2b}(dz + \cos\vartheta d\varphi)^2 + e^{2c}d\Omega^2, \quad (\text{A1})$$

where d, a, b and c are functions of t and R only, and where $d\Omega^2$ denotes the standard metric on S^2 . In order to do so, it is convenient to introduce the following orthonormal basis of one-forms,

$$\theta^0 = e^d dt, \quad \theta^1 = e^a dR, \quad \theta^2 = e^b (dz + \cos\vartheta d\varphi), \quad \theta^3 = e^c d\vartheta, \quad \theta^4 = e^c \sin\vartheta d\varphi.$$

With respect to this, the curvature two-form $\Omega_{ij} = \frac{1}{2}R_{ijkl}\theta^k \wedge \theta^l$ is

$$\begin{aligned} \Omega_{01} &= -\kappa \theta^0 \wedge \theta^1, \\ \Omega_{02} &= -\beta_0 \theta^0 \wedge \theta^2 - \beta_1 \theta^1 \wedge \theta^2 + (\dot{b} - \dot{c})e^{b-2c-d}\theta^3 \wedge \theta^4, \\ \Omega_{0A} &= -\gamma_0 \theta^0 \wedge \theta^A - \gamma_1 \theta^1 \wedge \theta^A + \frac{1}{2}(\dot{b} - \dot{c})e^{b-2c-d}\theta^2 \wedge \varepsilon_{AB}\theta^B, \\ \Omega_{12} &= -\beta_1 \theta^0 \wedge \theta^2 - \beta_2 \theta^1 \wedge \theta^2 + (b' - c')e^{b-2c-a}\theta^3 \wedge \theta^4, \\ \Omega_{1A} &= -\gamma_1 \theta^0 \wedge \theta^A - \gamma_2 \theta^1 \wedge \theta^A + \frac{1}{2}(b' - c')e^{b-2c-a}\theta^2 \wedge \varepsilon_{AB}\theta^B, \\ \Omega_{2A} &= -\frac{1}{2}(\dot{b} - \dot{c})e^{b-2c-d}\theta^0 \wedge \varepsilon_{AB}\theta^B - \frac{1}{2}(b' - c')e^{b-2c-a}\theta^1 \wedge \varepsilon_{AB}\theta^B + \delta_1 \theta^2 \wedge \theta^A, \\ \Omega_{34} &= (\dot{b} - \dot{c})e^{b-2c-d}\theta^0 \wedge \theta^2 + (b' - c')e^{b-2c-a}\theta^1 \wedge \theta^2 + \delta_2 \theta^3 \wedge \theta^4. \end{aligned}$$

Here, $A, B \in \{3, 4\}$, $\varepsilon_{34} = -\varepsilon_{43} = 1$, $\varepsilon_{33} = \varepsilon_{44} = 0$, a prime and a dot denote differentiation with respect to R and t , respectively, and

$$\begin{aligned} \kappa &= e^{-2d} [\ddot{a} + \dot{a}(\dot{a} - \dot{d})] - e^{-2a} [d'' + d'(d' - a')], \\ \beta_0 &= e^{-2d} [\ddot{b} + \dot{b}(\dot{b} - \dot{d})] - e^{-2a} b' d', \\ \beta_1 &= e^{-a-d} [\dot{b}' + \dot{b}(b' - d') - \dot{a} b'], \\ \beta_2 &= e^{-2a} [b'' + b'(b' - a')] - e^{-2d} \dot{a} \dot{b}, \\ \gamma_0 &= e^{-2d} [\ddot{c} + \dot{c}(\dot{c} - \dot{d})] - e^{-2a} c' d', \\ \gamma_1 &= e^{-a-d} [\dot{c}' + \dot{c}(c' - d') - \dot{a} c'], \\ \gamma_2 &= e^{-2a} [c'' + c'(c' - a')] - e^{-2d} \dot{a} \dot{c}, \\ \delta_1 &= e^{-2d} \dot{b} \dot{c} - e^{-2a} b' c' + \frac{1}{4} e^{2b-4c}, \\ \delta_2 &= e^{-2d} \dot{c}^2 - e^{-2a} c'^2 - \frac{3}{4} e^{2b-4c} + e^{-2c}. \end{aligned}$$

The corresponding components of the Ricci tensor are obtained from $R_{ij} = \Omega^k_i(e_k, e_j)$, where e_j , $j = 0, 1, \dots, 4$, is the Fünfbein corresponding to the orthonormal basis $\theta^0, \theta^1, \dots, \theta^4$ of one-forms. Explicitly, we find

$$R_{11} = e^{-2d} [\ddot{a} + \dot{a}(\dot{a} + \dot{b} + 2\dot{c} - \dot{d})] - e^{-2a} [d'' + b'' + 2c'' + d'(d' - a') + b'(b' - a') + 2c'(c' - a')], \quad (\text{A2})$$

$$R_{22} = e^{-2d} \left[\ddot{b} + \dot{b}(\dot{a} + \dot{b} + 2\dot{c} - \dot{d}) \right] - e^{-2a} [b'' + b'(b' + 2c' + d' - a')] + \frac{1}{2} e^{2b-4c}, \quad (\text{A3})$$

$$R_{33} = R_{44} = e^{-2d} \left[\ddot{c} + \dot{c}(\dot{a} + \dot{b} + 2\dot{c} - \dot{d}) \right] - e^{-2a} [c'' + c'(b' + 2c' + d' - a')] - \frac{1}{2} e^{2b-4c} + e^{-2c}, \quad (\text{A4})$$

$$R_{01} = R_{10} = -e^{-a-d} \left[\dot{b} + 2\dot{c}' - d'(\dot{b} + 2\dot{c}) + b'(\dot{b} - \dot{a}) + 2c'(\dot{c} - \dot{a}) \right], \quad (\text{A5})$$

$$R_{00} = 2G_{00} - R_{11} - R_{22} - R_{33} - R_{44}. \quad (\text{A6})$$

Here, G_{00} refers to the 00 components of the Einstein tensor, which is

$$G_{00} = e^{-2d} \left[\dot{a}(\dot{b} + 2\dot{c}) + \dot{c}(\dot{c} + 2\dot{b}) \right] - e^{-2a} [b'' + 2c'' + (b' - a')(b' + 2c') + 3c'^2] - \frac{1}{4} e^{2b-4c} + e^{-2c}. \quad (\text{A7})$$

The remaining components of R_{ij} are identically zero.

Using the fact that the metric is $SO(3)$ symmetric and homogeneous in the z direction, several curvature invariants can be defined. For this, consider the five-metric ds^2 in Eq. (A1), the orbit three-metric

$$d\tilde{s}^2 = -e^{2d} dt^2 + e^{2a} dR^2 + e^{2b} dz^2$$

and the projection thereof on the spaces orthogonal to the Killing field ∂_z

$$d\tilde{s}^2 = -e^{2d} dt^2 + e^{2a} dR^2.$$

The Kretschmann invariants $I = R_{ijkl} R^{ijkl}$ with respect to these metrics are

$$\tilde{I} = 4\kappa^2, \quad (\text{A8})$$

$$\bar{I} = 4[\kappa^2 + \beta_0^2 - 2\beta_1^2 + \beta_2^2], \quad (\text{A9})$$

$$I = 4\left[\kappa^2 + \beta_0^2 - 2\beta_1^2 + \beta_2^2 + 2\gamma_0^2 - 4\gamma_1^2 + 2\gamma_2^2 + 2\delta_1^2 + \delta_2^2 - 3(\dot{b} - \dot{c})^2 e^{2(b-2c-d)} + 3(b' - c')^2 e^{2(b-2c-a)}\right]. \quad (\text{A10})$$

Finally, the twice contracted Bianchi identities $\nabla_i G^i_j = 0$ are

$$\dot{G}_{00} + (\dot{a} + \dot{b} + 2\dot{c})G_{00} + \dot{a}G_{11} + \dot{b}G_{22} + \dot{c}(G_{33} + G_{44}) = e^{d-a} [G'_{01} + (b' + 2c' + 2d')G_{01}], \quad (\text{A11})$$

$$\dot{G}_{01} + (2\dot{a} + \dot{b} + 2\dot{c})G_{01} = e^{d-a} [G'_{11} + d'G_{00} + (b' + 2c' + d')G_{11} - b'G_{22} - c'(G_{33} + G_{44})]. \quad (\text{A12})$$

APPENDIX B: TANGHERLINI SOLUTION AND INVARIANTS

Tangherlini's solution [14] in five dimensions reads

$$ds^2 = -\left(1 - \frac{C}{r^2}\right) dt^2 + \left(1 - \frac{C}{r^2}\right)^{-1} dr^2 + r^2 d\Omega_3^2 \quad (\text{B1})$$

with C related to the ADM mass by

$$M_{ADM} = \frac{3\pi}{8} C. \quad (\text{B2})$$

For the curvature invariants, we find $\kappa = 3C/r^4$, $\beta_0 = \beta_2 = \gamma_0 = \gamma_2 = \delta_1 = \delta_2 = C/r^4$, $\beta_1 = \gamma_1 = 0$, and so the curvature invariants \tilde{I} , \bar{I} and I defined in appendix A are

$$\tilde{I} = 36 \frac{C^2}{r^8}, \quad \bar{I} = 44 \frac{C^2}{r^8}, \quad I = 72 \frac{C^2}{r^8}.$$

At the event horizon, the following combinations are particularly simple: $J_N = \tilde{I} r_{EH}^4 / 36$, $K_N = \bar{I} r_{EH}^4 / 44$, $I_N = I r_{EH}^4 / 72$. Since $r_{EH}^2 = C$, $I_N = J_N = K_N = 1$ when evaluated at the horizon.

[1] H. Elvang, T. Harmark, and N.A. Obers. Sequences of bubbles and holes: new phases of Kaluza-Klein black holes. *JHEP*, 01003:003(1)–003(65), 2005.

- [2] H. Elvang and G.T. Horowitz. When black holes meet Kaluza-Klein bubbles. *Phys. Rev. D*, 67:044015(1)–044015(10), 2003.
- [3] G.T. Horowitz. Tachyon condensation and black strings. *JHEP*, 0508:091(1)–091(16), 2005.
- [4] J. He and M. Rozali. On bubbles of nothing in AdS/CFT. [hep-th/0703220](http://arxiv.org/abs/hep-th/0703220), 2007.
- [5] V. Balasubramanian, K. Larjo, and J. Simon. Much ado about nothing. *Class. Quantum Grav.*, 22:4149–4170, 2005.
- [6] G.T. Horowitz and K. Maeda. Colliding Kaluza-Klein bubbles. *Class. Quantum Grav.*, 19:5543–5555, 2002.
- [7] B. Freivogel, G.T. Horowitz, and S. Shenker. Colliding with a crunching bubble. <http://arxiv.org/abs/hep-th/0703146>, 2007.
- [8] K. Copsey. Bubbles unbound: Bubbles of nothing without Kaluza-Klein. <http://arxiv.org/abs/hep-th/0610058>, 2006.
- [9] K. Copsey. Bubbles unbound II: AdS and the single bubble. <http://arxiv.org/abs/hep-th/0706.3677>, 2007.
- [10] O. Sarbach and L. Lehner. No naked singularities in homogeneous, spherically symmetric bubble spacetimes? *Phys. Rev. D*, 69:021901(1)–021901(5), 2004.
- [11] P. Olsson. Summation by parts, projections and stability. I. *Mathematics of Computation*, 64:1035–1065, 1995.
- [12] D. Nielsen, L. Lehner, O. Sarbach, and M. Tiglio. Recent analytical and numerical techniques applied to the Einstein equations. *Lect. Notes Phys.*, 692:223–249, 2006.
- [13] P. T. Chrusciel, E. Delay, G. J. Galloway, and R. Howard. Regularity of horizons and the area theorem. *Annales Henri Poincaré*, 2:109–178, 2001.
- [14] F. R. Tangherlini. Schwarzschild field in n dimensions and the dimensionality of the space problem. *Nuovo Cim.*, 27:636–651, 1963.